Al-Rafidain Journal of Engineering Sciences
Journal homepage https://rjes.iq/index.php/rjes
ISSN 3005-3153 (Online)

Study the effect of changing the length of the triangle leading edge of a flat plate on the separation distance of the flow

HANAN SALIM AL-JEBORY[1],*, HAYDER AZEEZ DIABIL[2]

[1,2]Mechanical Department, College of Engineering, Kufa University, Iraq

ARTICLE INFO

Article history:
Received 29 September 2023
Revised 30 September 2023
Accepted 21 October 2023
Available online 21 October 2023

Keywords:
Shedding frequency
Triangle leading edge
separation distance
flat plate

ABSTRACT

There are two primary facets of the separated-reattached in this study. Translational flow from a flat plate with a triangle edge in three dimensions, simulated with a huge vortex using the Ansys Fluent CFD simulation. The consistency of the edge is the study's outcome as it looked at how to use an isosceles triangular edge to shorten the flow's separation length. Three different lengths of cases were recorded. We found that the mean length of the reattachment was 4 cm in the first case, where the triangle's edge length was 0.5 cm. We measured the mean length of the reattachment in the second example, where the triangle's edge was 1 cm, and in the third case, when the triangle's edge measured 1.5 cm, we found that the mean length of the reattachment was (1.8 cm). Based on our analysis, the optimal case is the third one. As the edge length increases, the mean reattachment length decreases.

1. Introduction

Separated boundary layers are important to understand because their drag, lift, and heat transfer rates change dramatically in many real-world engineering situations. This is true whether the flow is internal (around airfoils, projectiles, vehicles, and buildings) or external (in diffusers, etc.). Transition in the separated boundary layer, which comprises a change from laminar to turbulent, is more challenging than transition in connected flow, where features of the separated layer transition are still quite challenging [1]. Either a strong, unfavourable pressure gradient or the presence of an internal obstruction causes the flow to separate. The first separation case's separation and reattachment locations shift when the flow parameters change because the boundary layer's momentum is insufficient to overcome the pressure gradient [2]. Because of this, instability in aerospace structures has been experimentally shown to reduce aerodynamic performance and create potentially dangerous dynamic structural loading [3] and [4].

Due to increases drag force, which lowers these systems' efficiency and stability, separation bubbles are parasites in aerodynamic applications. Therefore, it has been experimentally proven that instability develops in aerospace structures that degrade aerodynamic performance and result in potentially dangerous dynamic structural loading [3] and [4]. Laminar,

* Corresponding author.
E-mail address: Hanansalim9188@gmail.com

This work is licensed under https://creativecommons.org/licenses/by-nc-sa/4.0/

turbulent, and transitional flows are the three different kinds of separated-reattached flows. Thus, instability outcomes in aerospace structures have experimentally shown to degrade aerodynamic performance as well as generate potentially dangerous loading of dynamic structural [3] and [4]. A laminar flow separates into a laminar free shear layer in a transitional separated-reattached flow when the Reynolds number is reasonably low. When a laminar layer separates, it becomes unstable and is prone to changing into a turbulent flow that attaches to a solid surface. The separation bubble in this type of separated-reattached flow is vulnerable to instability because it is sensitive to even minor changes in upstream flow [4] and [5]. The various shedding frequency patterns and the production of large-scale structures are two key aspects of the transitional separated reattached flow, both of which are discussed in detail in this article. Low frequency mode, characteristic (regular) frequency shedding mode, and selected high frequency mode are the three frequency modes of separated-reattached flows that have been studied extensively in the literature. The low-frequency mode, which is related to the dynamics of separation bubble creation and decay, is also referred to in the literature as low-frequency shear layer flapping. The frequency of the sep's large-scale structural characteristic shedding The large-scale structural characteristic shedding frequency from the separation bubble's free shear layer is understood as the characteristic frequency shedding mode. It has been discovered that the low-frequency motion in the shear layer is related to the selective high-frequency shedding from the separated shear layer [8].

Numerous investigations that looked at a turbulent separated-reattached flow on different geometries came to the conclusion stated by Cherry et al. [7]. In a backward-facing step flow, there are more shedding frequency modes besides the standard one. Lee and Sung [9] also demonstrated the low-frequency shear layer flapping near the separation line. On a flat plate with a long central splitter plate, this phenomenon was discovered in separated flow [10] and [11]. The power spectra in [12] did not, however, detect any dominating modes of frequencies for identical flow configurations. On the other hand, numerical investigations by Yang and Voke [13] and Ducoine et al. [14] could refute Cherry et al. [7]'s assertion that low-frequency shear layer flapping was a necessary requirement for a totally turbulent separation. Separated flow is laminar and experiences low-frequency shear layer flapping with a value of 0.104 Uo/xR close to the separation line, as discovered by Yang and Voke [13] for a flat plate with a semicircular leading edge that forms a transitional separated-reattached flow. The authors claim that significant vortex shedding that occurred at a lower frequency is what gave rise to this phenomenon. The results of this investigation showed that the normal shedding frequency ranged from 0.35 U_0/XR to 1.14 U_0/XR. 0.77 U_0/XR was the predicted average frequency. The initiation of turbulence in a wing section was investigated by Ducoine et al. [14]. The spectra showed that the laminar separation section's shear layer flapping was predicted to have an expected magnitude with a Setrouhal number value of 0.08. The relationship between the Setrouhal number values of 0.12 and 0.248 and the two distinct frequencies at which the large-scale structures lose their bonds with the separating bubble was proven in the experiment. Tafti and Vanka [8] postulated that the separation bubble's

cyclical expansion and contraction caused the low-frequency shear layer flapping they observed, with a magnitude of 0.15 U0/XR, in a turbulent separated shear layer on a blunt flat plate. They identified a distinct high-frequency mode and found that its period was equivalent to that of the low-frequency instability. With the aid of an SD7003 wing section and the influence of an unfavorable pressure gradient, Ducoin et al. [14] investigated the instability processes of the transition to turbulence of a separated boundary layer flow over an airfoil at a low angle of attack. They showed how unstable separation bubble zones created and deformed two-dimensional Kelvin-Helmholtz rolls into C-shaped structures. When vortex filaments in the braid-breaking zone break, these structures are expelled from the separation bubble further downstream. Abdulla et al. [16] employed a two-dimensional surface-mounted obstruction and forward-facing step to depict the morphologies of transitional separated-reattached flow systems. By combining two Kelvin-Helmholtz rollers, a large roll was formed for both geometries. The lack of hairpin structures, which are categorized as coherent structures of separated-reattached flows on flat plates, was shown to create horseshoe vortices upon direct breakup of the massive rolls. More investigation is required to pinpoint the instability mechanism that led to the formation of three-dimensional structures as opposed to two-dimensional flat plates.

According to Spalart and Strelets [17], the Kilven-Helmholtz instability was the main mechanism of instability in the separated shear layer, and the lack of absolute instability was caused by insufficient reverse flow, which is required to promote the absolute instability.

In the first half of the separation bubble, McAuliffe and Yaras [18] also discovered that Kilven-Helmholtz rolls developed in the separated shear layer. The roll-up of spanwise vorticity into discrete vortical structures was caused, according to the authors, by the formation of a linear Tollmien-Schlichting instability following the separation. The authors observed that the transition sheared characteristics from viscous and inviscid instability processes, as the instability growth seen in their investigation resembled Kelvin-Helmholtz instability growth.

In the separated layer, Brinkerhoff and Yaras [19, 20] identified a relationship between viscous and inviscid instability processes. The Kelvin-Helmholtz instability, which is inviscid, is the predominant instability in the separated layer. The Tollmien-Schlichting instability mode in the connected boundary layer prior to the separation, according to the authors, created streamwise-oriented vortices that traveled into the separation bubble. There was a considerable interaction between these vortices and the inviscid Kelvin-Helmholtz instability in the transient zone, where they increased in the separated shear layer and created hairpin-like structures.

Gungor and Simens [21] and Karaca and Gungor [21] used the Q-criterion scheme, which has some similarities to the vorticity and pressure criteria, to demonstrate the impact of the span wise disturbance caused by surface roughness at the site of coherent structure breakdown. An unfavorable pressure gradient's effect on an aero foil caused the flow in these investigations to be a transitional-separated reattached flow. The aim of these studies was merely to focus on effect of surface roughness on the

breakdown location of large structures within the separation bubble. However, a description of coherent structures and their spatial and temporal evolution was not given in these studies.

According to Yang and Abdulla [22], the Kelvin-Helmholtz rolls themselves develop into three-dimensional hairpin and rib-like structures in the reattached turbulent boundary layer and near the reattachment zone. Based on their numerical simulation, the authors deduced that the helical instability, which is connected to the helical pairing of vortices and was thought to be a secondary instability mechanism of the transition, was most likely what caused the change from two-dimensional to three-dimensional coherent structures. According to Yang and Abdulla [22],

Niew [23] estimated that the absolute instability for backward-facing step flows occurs at a reverse flow intensity of greater than 20%. According to Hammond and Redekopp (1998), absolute instability occurs when the separation bubble's strength of the reverse flow reaches (approximately) 30% of the environmental stream speed. With a transitional separated flow on a NACA 0018 aero foil, Kurelek et al. [24] observed span wise undulations of span wise rolls that shed from the separated layer.

Kiya and Sasaki [25] showed in their experimental study that turbulent separated-reattached flow was characterized by three-dimensional hairpin vortex for a comparable shape but with a higher Reynolds number. There were two oppositely revolving pairs of vortices here.

Pradeep Singh and S. Sarkar (2021) address the issue of the excitation of a separated boundary layer near the leading edge due to surface roughness. Using a model airfoil with a semicircular leading edge, experiments are conducted at a Reynolds number (Rec) of 1.6 *105 and a free stream turbulence (fst) of 1.2%. The three rough surfaces, which are determined from the velocity profile at a site for downstream of reattachment.

In Eljack et al (2021) The flow field around a NACA-0012 airfoil is examined at Reynolds number, Mach number, and various angles of attack near stall in this study to determine the effects of angle of attack on the characteristics of the laminar separation bubble (LSB), its associated low-frequency flow oscillation (LFO), and the flow field.

Abdulla and Yang [26] found that their transitional separated-reattached flow had a selectively high frequency at a higher Reynolds number (6.5 * 103) based on the input velocity and flat plat thickness.

Abdulla and Yang [2] found that there is a high frequency peak between 5 and 6.5 U0/XR, which is around seven times the typical shedding frequency (0.7 to 0.875 U0/XR), based on the spectra for the instantaneous pressure and velocity components.

The current study's main objective is to provide information on coherent structures and shedding frequencies. Using data from a large eddy simulation and the Ansys Fluent CFD toolbox, the transitional separated-reattached flow has been discussed in some detail.

2. Governing equations

The Navier-Stokes equations are the universal laws of physics for Newtonian fluids. Direct numerical simulation requires a very high-resolution numerical grid to catch all length scales, and a very small time step to capture all time scales in the

flow, in order to solve these equations. Given the varying durations required by different situations, this approach is costly and occasionally impractical for geometries with relatively high Reynolds numbers and/or complicated shapes. Large eddy simulation (LES) is used to lower the computational cost. This method directly computes massive eddies or large-scale motions (grid-scale) while modeling minor eddies (sub-grid-scale). The flow is divided into resolved (grid-scale) and unresolved (sub-grid-scale) parts using a spatial filter. Consequently, any current variable (g) can be written as:

$$g_i = \bar{g}\imath + g_i' \qquad (1)$$

$\bar{g}\imath$ is grid-scale and g_i' is sub gridscale.

If LES equations are solved using the finite volume approach, they are filtered in a top-hat-like manner by being integrated across control volumes, and the governing equations may be regarded of as being implicitly filtered. In this case, the local filter width is considered to be the same as the local grid spacing [21]. The Navier-Stokes equation and filtered continuity for the LES incompressible Newtonian flow

$$\frac{\partial \overline{u\imath}}{\partial x_j} = 0 \qquad (2)$$

$$\frac{\partial \overline{u\imath}}{\partial t} + \frac{\partial \overline{u\imath}\,\overline{u\imath}}{\partial x_j} = -\frac{1}{\rho}\frac{\partial p}{\partial x_i} + \nu\frac{\partial^2 \overline{u\imath}}{\partial x_j \partial x_j} - \frac{\partial \tau_{ij}}{\partial x_j} \qquad (3)$$

Where ui, uj (i, j = 1, 2, 3) are Cartesian form three velocity components, and p, ρ, τ and stand for pressure, density, and kinematic viscosity, respectively.

The grid-scale filter, a type of spatial filtering, is applied as indicated by the over bar notation. An eddy viscosity model is used to simulate the unresolved sub gride-scale stress.

The grid-scale strain rate tensor and the residual stress tensor (ij), which describes the impact of sub-grid-scale motions on the resolved fields, have a relationship that can be written as follows:

$$\tau_{ij} = -2\nu_t\overline{S\imath J} + \frac{1}{3}\delta_{ij}\tau_{kk} \qquad (4)$$

Where

$$\overline{S\imath J} = \frac{1}{2}\left(\frac{\partial \overline{u\imath}}{\partial x_i} + \frac{\partial \overline{uj}}{\partial x_i}\right) \qquad (5)$$

The Kronecker delta is δ_{ij} and it is 1 if i = j and 0 if i≠ j. Sij is the strain rate tensor at the grid scale, t is the sub grid-scale eddy viscosity, and τ_{kk} is the unrepresented isotropic component of the stress tensor, which is added to the pressure term. The third equation may be written as:

$$\frac{\partial \overline{u\imath}}{\partial t} + \frac{\partial \overline{u\imath}\,\overline{uj}}{\partial x_j} = -\frac{1}{\rho}\frac{\partial p^*}{\partial x_i} + \nu\frac{\partial^2 \overline{u\imath}}{\partial x_j \partial x_j} + 2\frac{\partial \nu_t \overline{S\imath J}}{\partial x_j} \qquad (6)$$

$$p^* = -\frac{1}{3}\rho\delta_{ij}\tau_{kk} \qquad (7)$$

The sub grid-scale eddy viscosity t in equation (6) needs to be solved. Smagorinsky put forth the earliest and most straightforward model to address the sub grid-scale eddy viscosity.

$$\nu_t = C\Delta^2|\bar{S}|.\ |\bar{S}| = \sqrt{2\overline{S\imath J}\ \overline{S\imath J}} \qquad (8)$$

To calculate the filter width, which is proportional to the cube of the cell volume, we use the model parameter C. (x, y, and z). The sub grid-scale stress (τij), derived from equations (4) and (8), can now be expressed as:

$$\tau_{ij} = -2C\Delta^2|\bar{S}|\overline{S\imath J} + \frac{1}{3}\delta_{ij}\tau_{kk} \qquad (9)$$

C = Cs^2, Cs is Smagorinsky constant, is the formula for the Smagorinsky model. The Smagorinsky constant's proper value specification is truly a contentious issue because none of the various values is perfect. However, the majority of publications in the literature make the assumption that the Smagorinsky constant is decreased to

0.1 for flow close to a solid wall and is considered to be 0.18 for isotropic turbulent flow.

There are numerous issues with the Smagorinsky model, including the fact that it is overly dissipative which makes it difficult to model varying flows and the need to modify the Smagorinsky constant [42, 43]. Germano et al. [44] created a dynamic sub grid-scale model to address these issues. In this model, the constant C is locally determined as the computations proceed in both space and time, avoiding the model coefficient from needlessly changing. In [44] and [45], the process of calculating the dynamic subgrid-scale coefficient is described.

3. Numerical solution

Figures 1, 2, and 3 depict the computational mesh and conceptual representation of the computational domain for the three-dimensional triangle edge flat plate. The computational mesh and conceptual representation of the computational domain for the three-dimensional triangle edge flat plate are presented in Figures 1, 2, and 3. Tables 1, 2, and 3 contain information on the computational domain for geometry shape. The separations between the inflow and outflow borders for each type are (x/D=4.5) and (x/D=20.5), respectively. The blockage ratio is 16, and the lateral margins are 8D (y = 0) distant from the midline. It has a domain span dimension of 4D.

A structured mesh of 19822084 cells arranged along the stream wise, wall-normal, and span wise directions is used to carry out the numerical simulation. For both geometries, the approximate frictional velocity is identical near the outflow boundary. Based on the downstream frictional velocity of the reattachment at x/D = 18, mesh cell sizes for both geometries are equal in terms of wall units. The cell size varies between $\Delta x^+=4.86$ and 26.417 in the stream wise direction and between $\Delta y^+=0.739$ and 30.49 in the wall-normal direction. In the span wise direction, a uniform grid size is employed, $\Delta z^+ = 4.88$, as shown in Figure 4.

Time iterations are performed using a time step of t = 210 -6 sec, which is equivalent to 0.001885 D/U0, where U0 represents a CLFmax number of 0.31 for the flat plate and is the inflow velocity for both geometries. The Courant-Friedrich-Lewy (CFL) number is obtained by combining the two numbers together.

$$CFL = \Delta t \left(\frac{|u|}{\Delta x} + \frac{|v|}{\Delta y} + \frac{|w|}{\Delta z}\right) \quad (10)$$

In order for the geometry to have a well-established transition and turbulent boundary layer, the simulation was run for about 100,000 time steps through the domain, or until the flow had reached a statistically stationary condition. The simulation took 1 sec (942.5 D/U0) in total. Considering that the plate is thick and that the inflow velocity is uniform, perpendicular to the plate, and 9.425 m/sec, the current study's Reynolds number is 6.5103. The outflow boundary uses a zero velocity gradient. At all walls, no-slip boundary criteria are used. There are free-slip boundary conditions applied to the lateral boundaries.

Periodic boundary conditions are used for triangle-edge flat plates in the span-wise direction, where it is presumed that the flow is statistically homogenous.

In the current investigation, a dynamic sub-grid scale model is used in a large eddy simulation run with Ansys Fluent. The FVM is used to discretize the governing equations for LES.

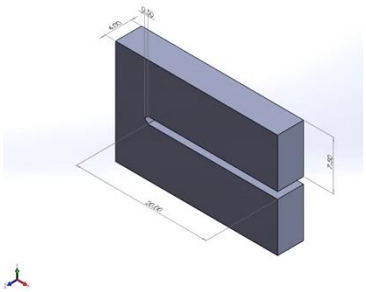

Figure 1: The three-dimensional domain conceptually represented triangle edge flat plate for case1_0.5.

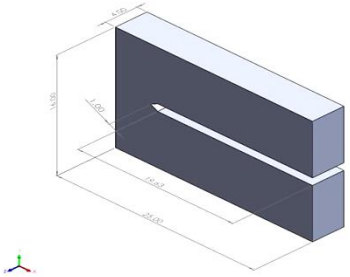

Figure 2: The three-dimensional domain conceptually represented triangle edge flat plate for case2_1.

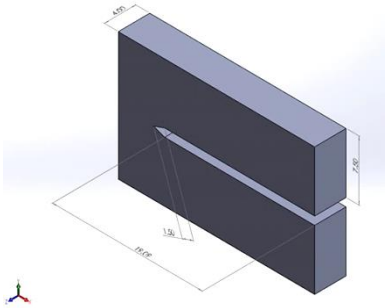

Figure 3:The three-dimensional domain conceptually represented triangle edge flat plate for case3_1.5.

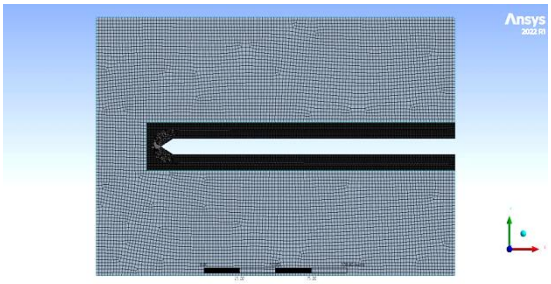

Figure 4: Mid-distance computational mesh in the span-wise orientation for geometry shape.

Table 1: Size for geometry shape.

LX	0.25 m
LY	0.16 m
LZ	0.04 m
Blockage ratio	16

Table 2: Domain size for geometry shape.

Triangle edge flat plate	
Thickness	1 cm
Length	20.5 cm
width	4 cm

Table 3: Domain size for geometry shapeof triangle edge for 3 cases.

Case No.	3D_case1	3D_case2	3D_case3
Thickness (D)	0.5 cm	1 cm	1.5 cm
Length (Ls)	20 cm	19.5 cm	19 cm
Width	4 cm	4 cm	4 cm
Mean reattachment length(XR)	4 cm	2.6 cm	1.6 cm

4. Results and discussion

The flat plate's geometry and Reynolds number in the current investigation are comparable to those in Castro and Epik's experimental study [28] and Yang and Abdalla's numerical study [27]. In [28], a flap was employed to limit the duration of the reattachment, and the blockage ratio was larger than the current blockage ratio. The primary goal of Castro and Epik's experimental work [28] was to investigate the turbulent boundary layer following reattachment. Findings from another experimental investigation in [6] were used here because the separation bubble's findings in this experiment were only partially successful.At a Reynolds number (26103) larger than the present Reynolds number, Kiya and Sasaki [6] investigated turbulent divided-reattached flow on a flat plate with a blunt leading edge. There was no transition in this experimental study, and the blockage ratio was greater than the previous blockage ratio.

The mean reattachment duration has a considerable impact on the separated-reattached flow (XR). The first grid point away from the wall at which the average streamwise velocity equals zero (Um = 0), found streamwise, is the mean reattachment point, according to Le et al. [49]. Figure 5 displays the geometry at the first cell, which is farthest from the wall along the streamwise direction, as well as the streamwise mean velocity profile. The triangle-edge flat plate's mean reattachment length for three cases (XR = 4D) for case 1, (XR = 2.6D) for case 2, and (XR = 1.6D) for case 3 is amply demonstrated.

The measured mean reattachment length (7.7D) is longer than the current mean reattachment length (6D) for the flat plate case. This is a good agreement considering the flap's effects and Castro and Epik's and Epik's enhanced blockage ratio.

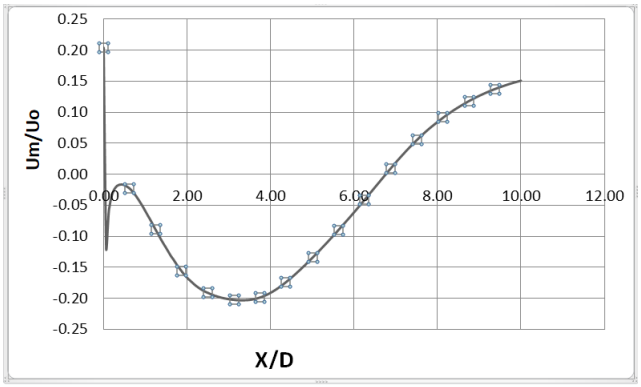

Figure 5: The mean streamwise velocity measured along the streamwise direction for the flat plate in the first cell farthest from the wall, normalized by the inflow velocity

Even while the current flat plate scenario's mean reattachment length is less than 6.7D as a predicted length of a separation bubble in [25], this is in good accord with numerous characteristics of the Ansys Fluent commercial code that is presently in use.

According to this measurement, the flat plate's mean reattachment length is greater than the mean reattachment length of Kiya and Sasaki's experimental study [6], which is 5.05D. The separated flow used in this experimental work, however, was totally turbulent and had a greater Reynolds number (26103) than the one now in use.

It's important to note that as the Reynolds number falls below 30×103, the separation bubble length increases [7]. In light of the experimental findings in [6], the current mean reattachment length is consistent. But the strong similarity between the present results and previous studies demonstrates that Ansys Flunt can accurately model the transitional separated-reattached flow. According to the literature review, the current study presents the results of a transitional separated-reattached flow over a three-dimensional geometry. The 3D_6cases mean values for flow variables are the result. A flat plate with a triangle edge also has the mean wall-normal velocity and other mean values of variables of transitional separated-reattached flow. This section analyzes the flow mean variables for all of the study's used geometries and provides a database for further research to corroborate findings. Figures, and shows the mean stream wise velocity distribution along the stream wise direction at the first cell away from the wall for the three different 3D cases.

The distribution of the value of the mean stream-wise velocity at the first cell away from the wall along the stream-wise direction for 3D_case1 is represented in Figure 7 in an equilateral triangle edge (Note that the edge of the triangle is equal to 0.5 cm). It is evident that for 3D-case1, XR = 4D is the mean reattachment length.

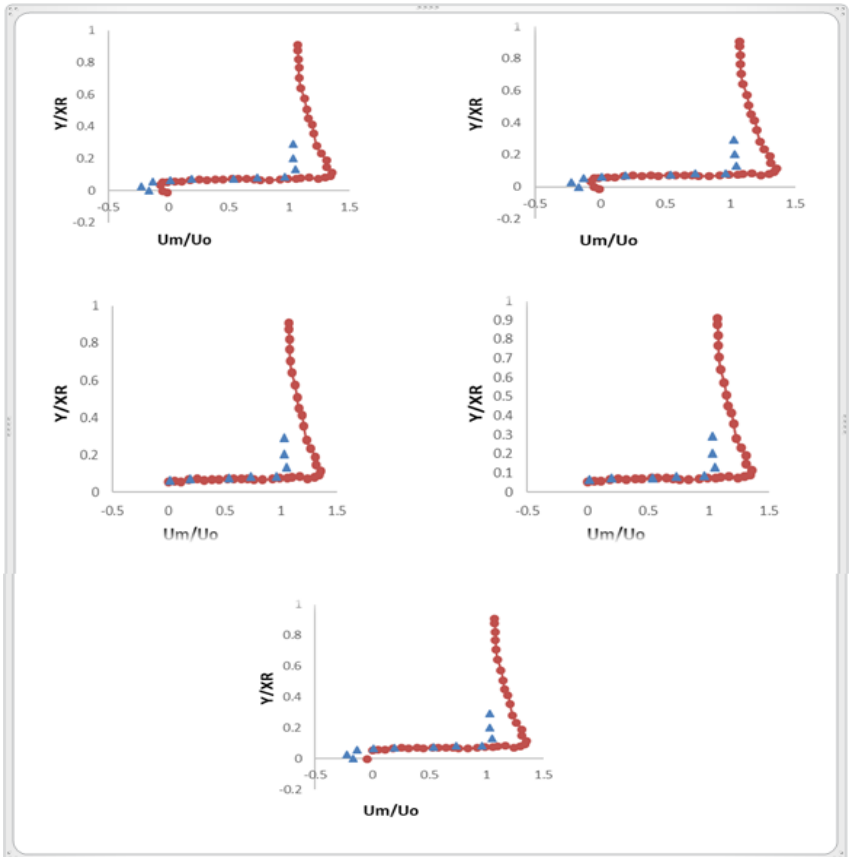

Figure 6: Profile of mean stream wise velocity, current results as solid line, Yang and Abdulla results as circles and Kiya and Sasaki results as triangles.

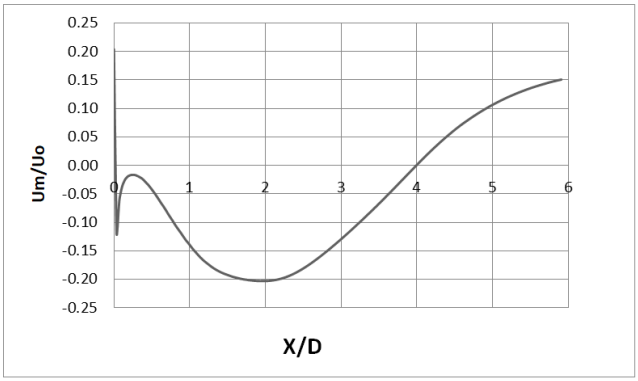

Figure 7: Profile of the mean streamwise velocity along the streamwise direction at the first cell away from the wall for 3D case1 normalized by the inflow velocity.

The distribution of the value of the mean stream-wise velocity at the first cell away from the wall along the stream-wise direction for 3D_case1 is represented in Figure 8 in an equilateral triangle edge (note that the edge of the triangle is equal to 1 cm. It is evident that for 3D-case1, XR = 2.8D is the mean reattachment length.

It is worth pointing out that the symbol (XR) shown in all figures of the current study denotes different values depending on the geometry, i.e., XR is 6.77D for the flat plate figures, XR=4D for 3D_case1, XR=2.8D for 3D_case2, XR=1.6D for 3D_case3

Figure 10 displays the mean stream-wise velocity profile for 3D_case1. The minimal mean stream-wise velocity in the vicinity of the wall and inside the recirculation zone for three-dimensional geometry is about equivalent to that for the flat plate. However, in the region between X/XR = 0.6 and X/XR = 0.8, the minimal mean stream-wise velocity lies between $-0.29U_0$ and $-0.31U_0$. Despite the fact that this for three-dimensional geometry the minimum mean stream-wise velocity for the flat plate is a little lower. According to the current research, the geometry's nature has no discernible impact on the amount of back flow.

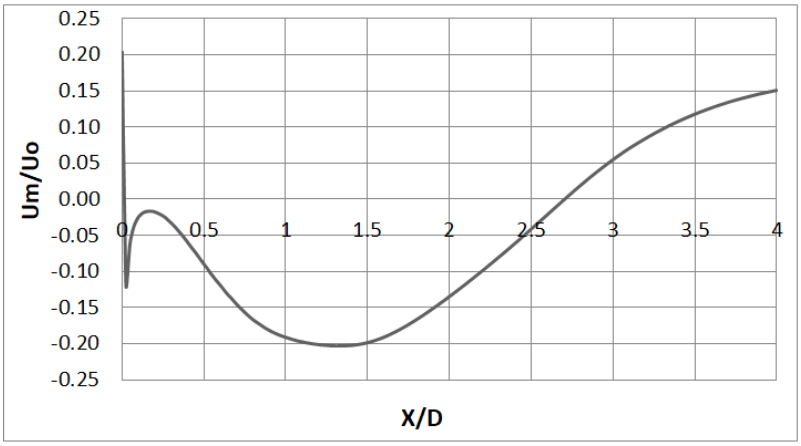

Figure 8: Profile shows the mean streamwise velocity along the streamwise direction for the first cell away from the wall for 3D case2 normalized by the inflow velocity.

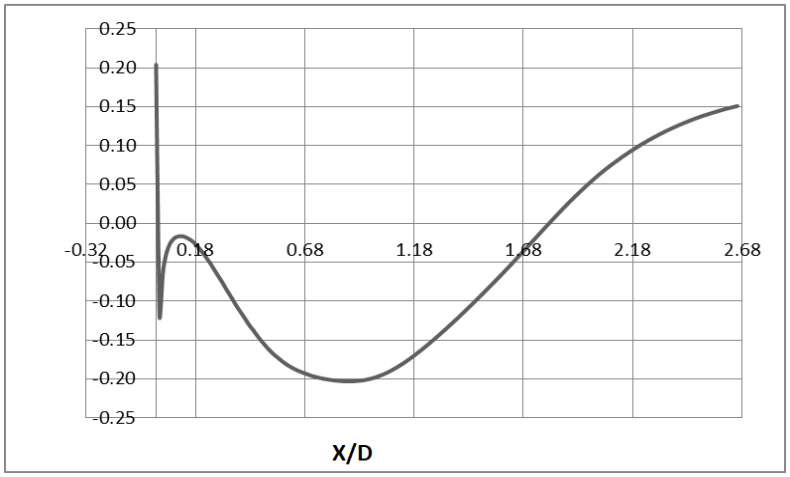

Figure 9: Profile shows the mean streamwise velocity along the streamwise direction at the first cell away from the wall, normalized by the inflow velocity for 3D case3.

The mean stream-wise velocity profile for 3D_case2 is shown in Figure (11). For three-dimensional geometry, the minimal mean stream-wise velocity close to the wall and inside the recirculation zone is about comparable to that for the flat plate. The minimal mean stream-wise velocity, on the other hand, lies in the range between $-0.3U_0$ and $-0.31U_0$ between X/XR = 0.6 and X/XR = 0.8. Although this is for three-dimensional geometry, the flat plate's minimum mean stream-wise velocity is a little lower. The nature of the geometry has no appreciable effect on the quantity of

backflow, according to the present studies.

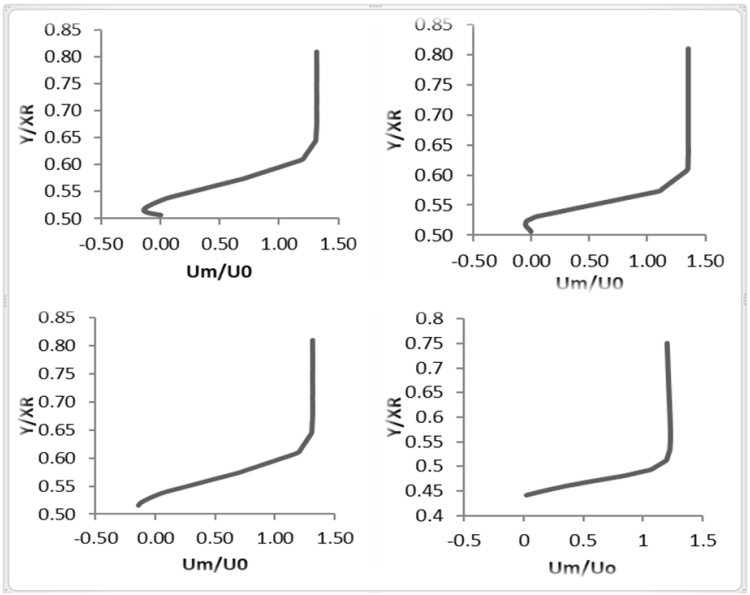

Figure 10: Mean stream wise velocity profiles of the flow for case 1.

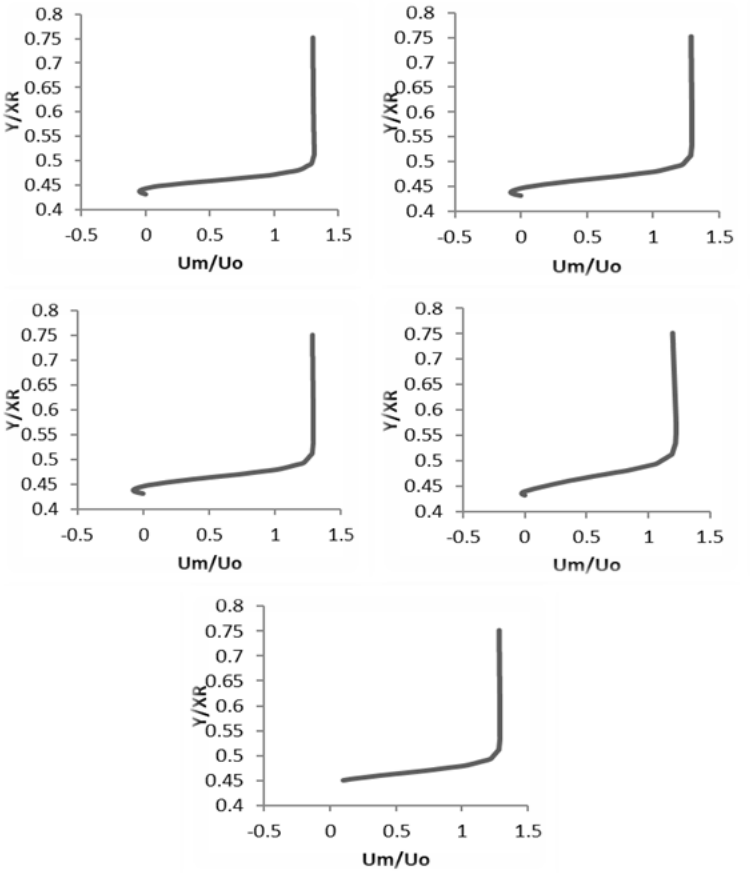

Figure 11: Mean stream wise velocity profiles of the flow for case 2.

The mean stream-wise velocity profile for 3D_case3 is shown in Figure 12. For three-dimensional geometry, the minimal mean stream-wise velocity close to the wall and inside the recirculation zone is about comparable to that for the flat plate. The minimal mean stream-wise

velocity, on the other hand, lies in the range between $-0.33U_0$ and $-0.32U_0$ between X/XR = 0.6 and X/XR = 0.8.

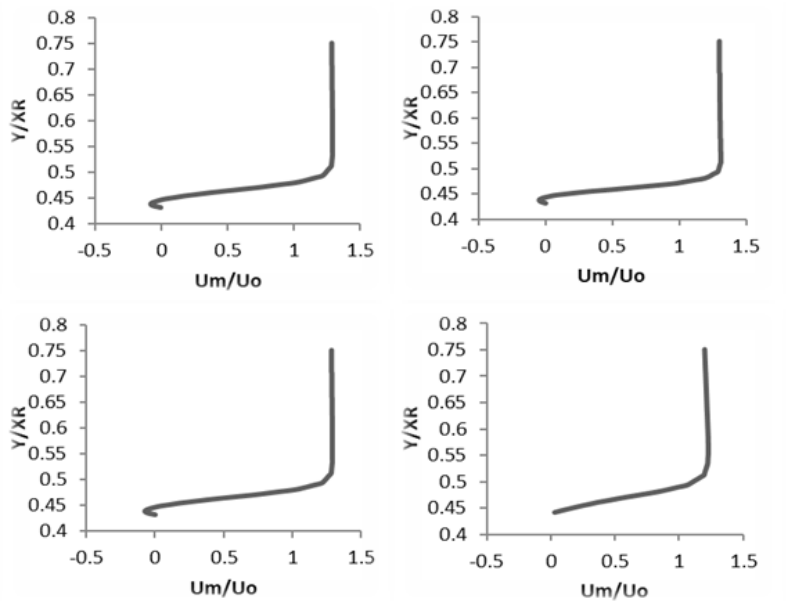

Figure 12: Mean stream wise velocity profiles of the flow for case 3.

When the three scenarios' outcomes were compared, it was discovered that the situation where the triangle's edge is equal to 1.5 cm is the best case. The mean reattachment length reduces as the edge length rises. As shown in Figure 13.

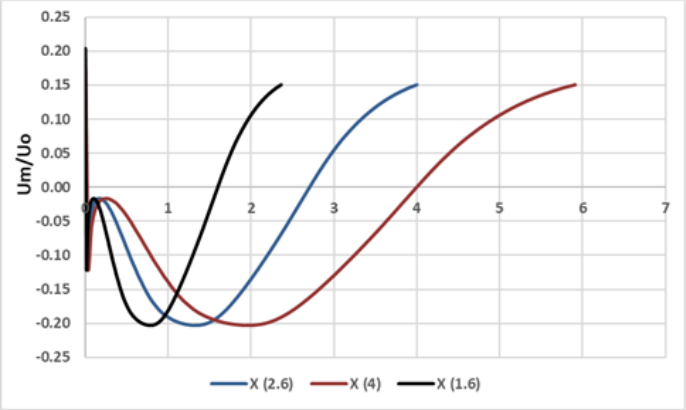

Figure 13: Profile of stream wise normalized mean velocity by inflow velocity at the first cell from the wall along the stream wise direction: black line for edge triangle flat plate1.5cm, Blue line for edge triangle flat plate 1cm and Red line for edge triangle

Figures 14, 15, and 16 show the time-averaged velocity streamlines, velocity vectors, and stream-wise velocity contours for the triangular edge of the flat plate in 3D_cases 1, 2, and 3, respectively, at the midpoint of the span-wise direction (z/D = 2).

The separation bubble in question is equal to a separation bubble for a constant laminar flow that has been detached and then reattached with various reattachment times. A single separation bubble is clearly seen to begin at the leading edge at x/D = 0

and finish downstream at about x/D = 6.77D for the flat plate, x/D = 4D for the 3D case 1, x/d = 2.6D for the 3D case 2, and X/d = 1.6D for the 3D case 3. The separating bubble for the flat plate is substantially larger in height and length than it is for any of the three-dimensional geometries.

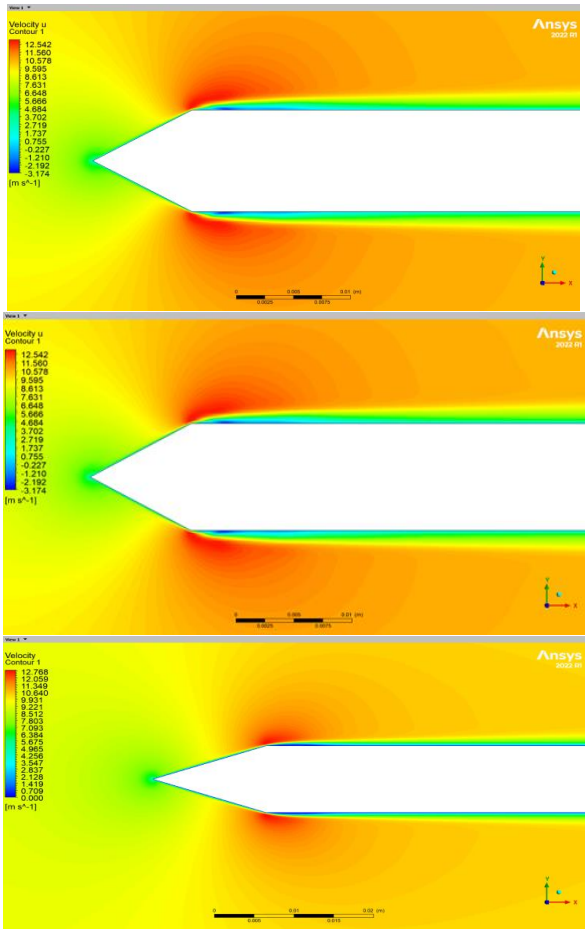

Figure 14: Stream-wise velocity contours for 3D_case1, 2, 3.

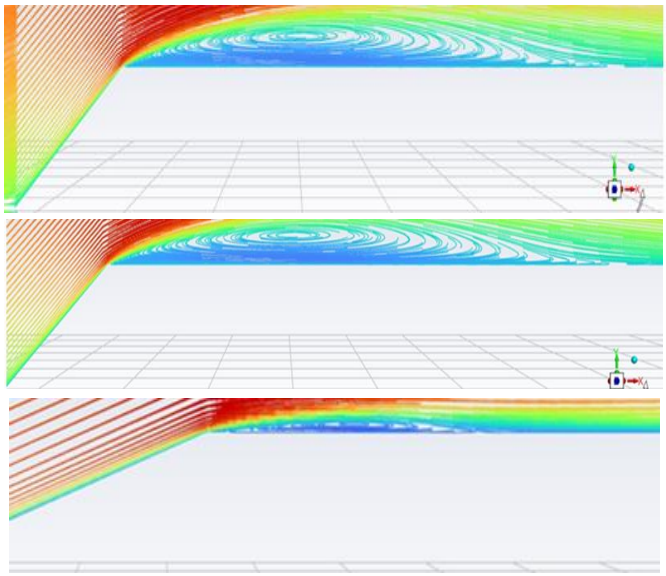

Figure 15: Mean velocity stream line for 3D_case1, 2, 3.

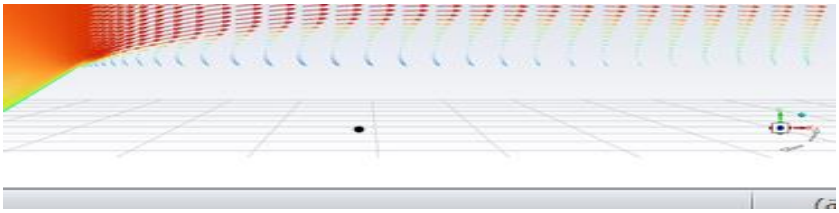

Figure 16: Velocity vector for triangle edge flat plate.

5. Conclusions

The properties of a transitional separated-reattached flow over six case studies have been investigated in this thesis by employing three geometrical shapes with two disturbance levels in the incoming flows. The geometries are a blunt flat plate (with an infinity aspect ratio) and two three-dimensional geometries characterized by two different aspect ratios (1 and 2). Low level of intensity of free stream turbulence (< 0.2%) and high level of intensity of free stream turbulence (3.7%) are applied in the current study. The numerical simulations are carried out by the commercial ANSYS tool box employing LES with the dynamic localization SGS. The good agreement obtained from the comparison among the current OF code results and the available experimental data and simulated results for the flat plate with NFST and FST is encouraging in terms of the simulation results obtained for transitional separated reattached flow over three-dimensional geometries. To the best of the author's knowledge, there are no published results for separated-reattached flow over a three-dimensional geometry. Therefore, the current study is the first to investigate such a flow with low and also high levels of intensity of free stream turbulence over three-dimensional geometries with different aspect ratios.

The separation bubble mean length is 6D for the flat plate which reduces to 4D for 3D_case1, 2.7D for 3D_case2and 1.8D for 3D_case3. This indicates that the separation on the flat plate is longer than that on the three-dimensional geometries. In addition, there is no strong effect associated with changing the aspect ratio of the three-dimensional geometry on the mean reattachment length.

References

[1] Taghinia, J., Rahman, M., and Siikonen, T., Large Eddy Simulation of Flow Past a Circular Cylinder with a Novel Sub-Grid Scale Model, European Journal of Mechanics B/Fluids, Vol. 52, pp. 11-18.X1,2015.

[2] Alving A. E. and Fernholz H. H., Turbulence Measurements around a Mild Separation Bubble and Downstream of Reattachment, Journal of Fluid Mechanics, Vol. 322, pp. 297-328,1996.

[3] Schreck, S. J. and Robinson, M. C., Horizontal Axis Wind Turbine Blade Aerodynamics in Experiments and Modeling, IEEE Transactions on Energy Conversion, Vol. 22, No. 1, pp. 61-70,2007.

[4] Bak, C., Madsen, H. A., Fuglsang, P., and Rasmussen, F., Observations and Hypothesis of Double Stall, Wind Energy, Vol. 2, No. 1, pp. 195-210,1999.

[5] Rist, U. and Augustin, K., Control of Laminar Separation Bubbles Using Instability Waves, AIAA Journal, Vol. 44, No. 10, pp. 2217- 2223,2006.

[6] Kiya, M. and Sasaki, K., Structure of a Turbulent Separation Bubble, Journal of Fluid Mechanics, Vol. 137, pp. 83–113,1983.

[7] Cherry, N. J., Hillier, R., and Latour, M.E.M.P., Unsteady Measurements in a Separated and Reattaching Flow, Journal of Fluid Mechanics, Vol. 144, pp. 13-46,1984.

[8] Tafti, D. K. and Vanka, S. P., A Three Dimensional Numerical Study of Flow Separation and Reattachment on a Blunt

Plate, Physics of Fluids, Vol. 3, No. 12, pp. 2887-2909,1991.

[9] Lee, I., and Sung, H. J., Characteristics of wall pressure fluctuations in separated and reattaching flow over a backward-facing step, Exp. Fluid, Vol. 30,pp. 262-272,2001.

[10] Hudy, L. M., Naguib, A. M., Humphreys, W. M., Wall-pressure-array measurements beneath a separating/reattaching flow region, Phys. Fluid, Vol. 15, pp. 706-717,2003.

[11] Castro, I. P., Haque, A., The Structure of a Turbulent Shear Layer Bounding a Separation Region, Journal of Fluid Mechanics, Vol. 179, pp. 439-468,1987.

[12] Ruderich, R. and Fernholz, H. H., An experimental investigation of a turbulent shear flow with separation, reverse flow and reattachment, Journal of Fluid Mechanics, Vol. 163, pp. 283–322,1986.

[13] Yang, Z., and Voke, P. R., Large-Eddy Simulation of Boundary Layer Separation and Transition at a Change of Surface Curvature, Journal of Fluid Mechanics, Vol. 439, pp. 305-333,2001.

[14] Ducoin, A., Loiseau, J., and Robinet, J., Numerical Investigation of the Interaction between Laminar to Turbulent Transition and the Wake of an Airfoil, European Journal of Mechanics B/Fluids, Vol. 57, pp. 231- 248,2016.

[15] Yang, Z., Numerical Study of Instabilities in Separated-Reattached Flows, Int. Journal of Comp. Meth. And Exp. Meas., Vol. 1, No. 2, pp. 116-131,2013

[16] Abdalla I. E., Yang, Z., and Cook, M., Computational Analysis and Flow Structure of a Transitional Separated-Reattached Flow over a Surface Mounted Obstacle and a ForwardFacing Step, International Journal of Computational Fluid Dynamics, Vol. 23, No. 1, pp. 25–57,2009.

[17] Spalart, P. R. and Strelets, M. K. Mechanisms of Transition and Heat Transfer in a Separation Bubble. J. Fluid Mech., 403: 329-349,2000.

[18] McAuliffe, B. R. and Yaras, M. I. Numerical Study of Instability Mechanisms Leading to Transition in Separation Bubbles. ASME Journal of Turbomachinery, 130: 021006,2008.

[19] Brinkerhoff, J. R. and Yaras, M. I. Interaction of Viscous and Inviscid Instability Modes in Separation-Bubble Transition. Physics of Fluids, 23, 124102,2011.

[20] Brinkerhoff, J. R. and Yaras, M. I. Direct Numerical Simulations of Transitional Separation-Bubble Development in Swept-Blade Flow Conditions. Journal of Turbomachinery, 135: 041006,2013.

[21] Gungora, A. G. and Simens, M. P. Transition to turbulence in a separated boundary layer with spanwise perturbations. IUTAM ABCM Symposium on Laminar Turbulent Transition, Science Direct, 14: 69-77, 2015.

[22] Lilly, D. K. , A proposed modification of the Germano subgrid-scale closure method. Phys. Fluids 1; vol. 4, pp. 633–635,1992. https://doi.org/10.1063/1.858280.

[23] Niew, T. R. The Stability of the Flow in a Laminar Separation Bubble. PhD thesis, University of Cambridge,1993.

[24] Kurelek, J. W., Burak, A. T., and Yarusevych, S.Three-Dimensional Vortex Development in a Laminar Separation Bubble formed over an Airfoil. 47th AIAA Fluid Dynamics Conference, 5-9 June 2017, Denver, Colorado: 3642,2017.

[25] Sasaki, K. and Kiya, M. Three-Dimensional Vortex Structure in a Leading-Edge Separation Bubble at Moderate Reynolds Numbers. Journal of Fluids Engineering, 113: 405-410,1991.

[26] Yang, Zhiyin & Abdalla, Ibrahim. On coherent structures in a separated/reattached flow. WSEAS Transactions on Fluid Mechanics 3:143-153. 3. 143-153, 2008..

[27] Yang, Z. and Abdalla, I. E. Effects of Free-Stream Turbulence on Large-Scale Coherent Structures of Separated Boundary Layer Transition. Int. J. Numer. Meth. Fluids, 49: 331-348,2005.

[28] Castro, L P. and Epik, E., Boundary Layer Development after a Separated Region,

Journal of Fluid Mechanics, Vol. 374, pp. 91- 116,1998.